Article

Cell Reports

Distinct Kinase-Independent Role of RIPK3 in CD11c$^+$ Mononuclear Phagocytes in Cytokine-Induced Tissue Repair

Graphical Abstract

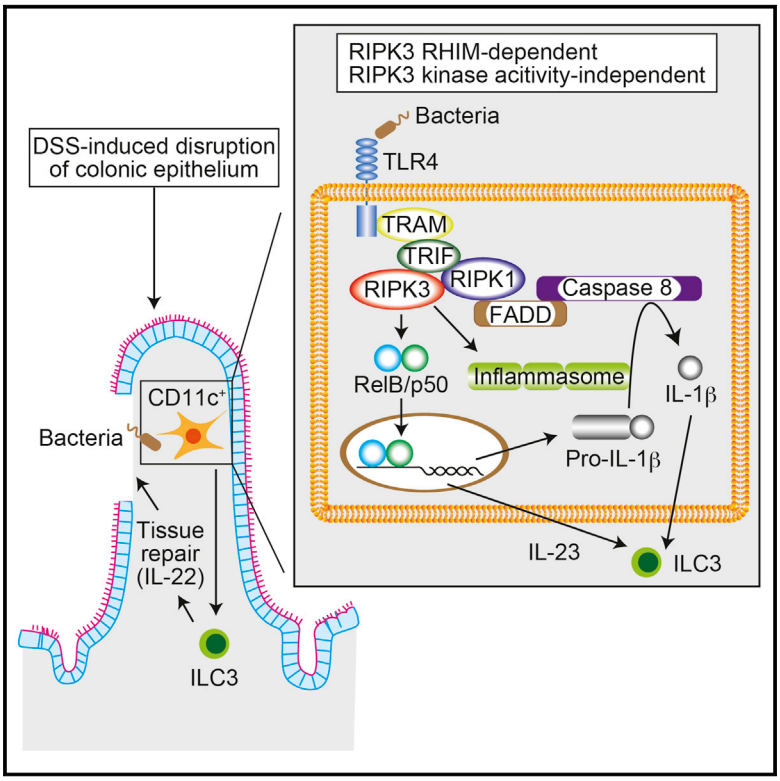

Authors

Kenta Moriwaki, Sakthi Balaji, John Bertin, Peter J. Gough, Francis Ka-Ming Chan

Correspondence

francis.chan@umassmed.edu

In Brief

Moriwaki et al. demonstrate that RIPK3 promotes cytokine production in CD11c$^+$ mononuclear phagocytes in an RHIM-dependent, but kinase-independent manner. This necroptosis-independent function of RIPK3 is crucial for tissue repair in response to intestinal injury.

Highlights

- Generation of RIPK3-GFP reporter mice to determine the in vivo expression of RIPK3
- Generation of RIPK3-ΔRHIM mutant mice to determine functions of the RIPK3 RHIM
- The RHIM is crucial for RIPK3-dependent necroptosis and cytokine expression
- Kinase-independent function of RIPK3 drives intestinal CD11c$^+$ MNPs cytokine production

Moriwaki et al., 2017, Cell Reports *18*, 2441–2451
March 7, 2017
http://dx.doi.org/10.1016/j.celrep.2017.02.015

Cell Reports
Article

Distinct Kinase-Independent Role of RIPK3 in CD11c$^+$ Mononuclear Phagocytes in Cytokine-Induced Tissue Repair

Kenta Moriwaki,[1,4] Sakthi Balaji,[1] John Bertin,[2] Peter J. Gough,[3] and Francis Ka-Ming Chan[1,5,*]
[1]Department of Pathology, Immunology and Microbiology Program, University of Massachusetts Medical School, Worcester, MA 01605, USA
[2]Pattern Recognition Receptor Discovery Performance Unit, Immuno-Inflammation Therapeutic Area, GlaxoSmithKline, Collegeville, PA 19422, USA
[3]Host Defense Discovery Performance Unit, Infectious Disease Therapy Area, GlaxoSmithKline, Collegeville, PA 19422, USA
[4]Present address: Department of Cell Biology, Osaka University Graduate School of Medicine, Osaka 565-0871, Japan
[5]Lead Contact
*Correspondence: francis.chan@umassmed.edu
http://dx.doi.org/10.1016/j.celrep.2017.02.015

SUMMARY

Receptor interacting protein kinase 3 (RIPK3) induces necroptosis, a type of regulated necrosis, through its kinase domain and receptor interacting protein (RIP) homotypic interaction motif (RHIM). In addition, RIPK3 has been shown to regulate NLRP3 inflammasome and nuclear factor κB (NF-κB) activation. However, the relative contribution of these signaling pathways to RIPK3-dependent inflammation in distinct immune effectors is unknown. To investigate these questions, we generated RIPK3-GFP reporter mice. We found that colonic CD11c$^+$CD11b$^+$CD14$^+$ mononuclear phagocytes (MNPs) expressed the highest level of RIPK3 in the lamina propria. Consequently, deletion of the RIPK3 RHIM in CD11c$^+$ cells alone was sufficient to impair dextran sodium sulfate (DSS)-induced interleukin (IL)-23 and IL-1β expression, leading to severe intestinal inflammation. In contrast, mice expressing kinase inactive RIPK3 were not hypersensitive to DSS. Thus, a key physiological function of RIPK3 is to promote reparative cytokine expression through intestinal CD11c$^+$ MNPs in a kinase- and necroptosis-independent manner.

INTRODUCTION

Necroptosis is a type of regulated necrosis induced by several cell surface immune receptors such as tumor necrosis factor (TNF) receptor (TNFR), Toll-like receptor (TLR) 3 (TLR3), TLR4, interferon receptor, and T cell receptor (Chan et al., 2015). Receptor interacting protein kinase 3 (RIPK3) is a cytosolic master regulator of necroptosis (Moriwaki and Chan, 2013). RIPK3 has an active serine-threonine kinase domain at the N terminus and a unique protein-protein interaction domain called the RIP homotypic interaction motif (RHIM) at the C terminus. Both kinase activity and RHIM are indispensable for necroptosis (Cho et al., 2009). RIPK3 interacts with other RHIM-containing proteins such as RIPK1 (Cho et al., 2009; He et al., 2009), Toll/interleukin-1 (IL-1) receptor domain-containing adaptor protein inducing interferon β (TRIF) (He et al., 2011), or DNA-dependent activator of interferon regulatory factor (DAI) (Upton et al., 2012). RHIM-RHIM interaction leads to amyloid-like conformational change and enhancement of RIPK3 kinase activity (Li et al., 2012). Activated RIPK3 phosphorylates the downstream adaptor MLKL (Sun et al., 2012), which triggers oligomerization and translocation of MLKL to the plasma membrane (Cai et al., 2014; Chen et al., 2014; Dondelinger et al., 2014; Wang et al., 2014).

Besides necroptosis, recent emerging evidence shows that RIPK3 also has necroptosis-independent functions (Moriwaki and Chan, 2014). For example, RIPK3 stimulates nuclear factor κB (NF-κB)-dependent *Il23p19* (*Il23a*) expression and pro-IL-1β processing downstream of TLR4 in bone marrow (BM)-derived dendritic cells (DCs) (BMDCs) (Moriwaki et al., 2014). Similar RIPK3-dependent processing of pro-IL-1β has also been observed in BM-derived macrophages (BMDMs) treated with Smac mimetics and/or caspase inhibitors (Kang et al., 2013, 2015; Lawlor et al., 2015; Vince et al., 2012). However, the relative contribution of necroptosis-dependent and -independent effects of RIPK3 in physiological inflammation has not been clearly elucidated.

Germline *Ripk3*-deficient mice have been used extensively to investigate the pathophysiological roles of RIPK3 (Chan et al., 2015). The resolution of inflammation in *Ripk3*$^{-/-}$ mice has often been attributed as a consequence of blocking necroptosis. Strikingly, RIPK3 has recently been shown to have paradoxical function in promoting injury-induced tissue repair (Godwin et al., 2015). In a mouse model of chemical-induced intestinal injury, RIPK3 facilitates expression of IL-23 and IL-1β, which in turn stimulates expression of the tissue repair cytokine IL-22. Thus, *Ripk3*$^{-/-}$ mice developed sustained injury and inflammation (Moriwaki et al., 2014, 2016). Based on these results, we asked whether RIPK3 promotes cytokine-induced tissue repair mainly through DCs. To achieve our goal, we generated "knock-in" mice expressing an RIPK3-GFP fusion reporter, as well as mice with tissue-specific deletion of the essential RHIM (*Ripk3*$^{\Delta R/\Delta R}$). Using the RIPK3-GFP reporter mice, we found that RIPK3 was highly expressed in intestinal CD11c$^+$CD11b$^+$CD14$^+$CD103$^-$

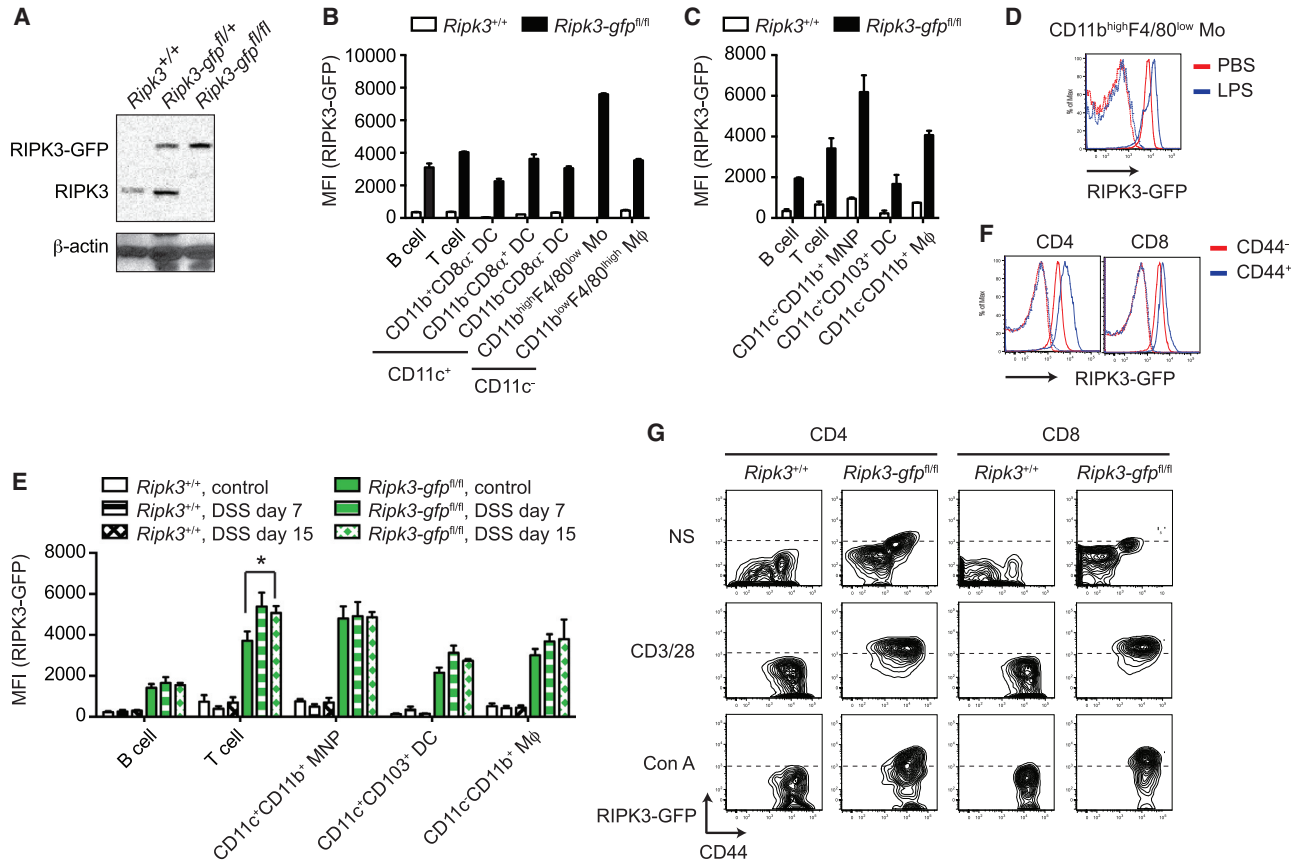

Figure 1. RIPK3 Is Highly Expressed in Colonic CD11c$^+$CD11b$^+$CD103$^-$ MNPs

(A) RIPK3-GFP and RIPK3 expression in MEFs of the indicated genotypes were examined by western blot.

(B and C) RIPK3 expression level in various subsets of immune cells in (B) spleen and (C) colonic lamina propria of *Ripk3-gfp*$^{fl/fl}$ reporter mice was determined by measuring the GFP fluorescence intensity using a flow cytometer (n = 2). CD19$^+$ and CD3$^+$ cells were defined as B and T cells, respectively. CD3$^-$CD19$^-$CD11c$^+$ cells were defined as DCs, except for colonic CD3$^-$CD19$^-$CD11c$^+$CD11b$^+$ cells, which were defined as MNPs. CD3$^-$CD19$^-$CD11c$^-$CD11b$^+$ cells were defined as macrophages (Mϕ), except for the CD3$^-$CD19$^-$CD11c$^-$CD11b^{hi}F4/80^{lo} cells, which were defined as monocytes (Mo).

(D) Spleen was harvested from *Ripk3*$^{+/+}$ (dashed line) and *Ripk3-gfp*$^{fl/fl}$ reporter mice (solid line) 15 hr after intraperitoneal injection of LPS (50 μg/mouse). Representative histogram of GFP fluorescence intensity in CD11b^{hi}F4/80^{lo} monocytes is shown.

(E) Mean fluorescence intensity (MFI) of the GFP fluorescence in various colonic lamina propria mononuclear cells from DSS-treated *Ripk3-gfp*$^{fl/fl}$ reporter mice is shown (n = 5–6).

(F) Representative histograms of the GFP fluorescence intensity in CD44^{hi} or CD44^{lo} splenic CD3$^+$CD4$^+$ or CD3$^+$CD8$^+$ T cells are shown.

(G) Splenocytes were stimulated with either anti-CD3 and anti-CD28 antibodies or concanavalin A (Con A) for 3 days. Representative FACS plots in CD3$^+$CD4$^+$ or CD3$^+$CD8$^+$ T cells were shown.

Results shown are mean ± SEM. *p < 0.05. See also Figures S1 and S2.

mononuclear phagocytes (MNPs). Deletion of RIPK3 RHIM in CD11c$^+$ cells fully recapitulated the severe intestinal inflammation observed in germline *Ripk3*$^{-/-}$ mice. In contrast, kinase inactive RIPK3 knock-in mice did not exhibit hypersensitivity in response to chemical-induced colitis. Collectively, these results reveal cell-type-specific functions of RIPK3 in inflammation as well as the importance of RHIM-RHIM-mediated interaction in biological responses beyond necroptosis.

RESULTS

Generation of RIPK3-GFP Reporter Mice

RIPK3 expression is often induced in tissues and cells during inflammation (Gautheron et al., 2014; Moriwaki et al., 2014; Vitner et al., 2014). To determine the physiological expression pattern of RIPK3 in quiescent and inflamed states, we generated RIPK3-GFP reporter mice in which the *Ripk3* gene was fused in-frame with the *eGfp* sequence at the end of the RIPK3 translated sequence (Figure S1A). Proper targeting of the *Ripk3* locus was confirmed by Southern blot analysis (Figures S1A–S1C). We confirmed that RIPK3-GFP and wild-type RIPK3 were expressed at similar levels in *Ripk3-gfp*$^{fl/+}$ mouse embryonic fibroblasts (MEFs) (Figure 1A). The percentage and number of T and B cells in the thymus and lymph node were normal in *Ripk3*$^{+/+}$ and *Ripk3-gfp*$^{fl/fl}$ mice (Figures S1D and S1E and data not shown). In addition, the composition of BM cells was unchanged in *Ripk3-gfp*$^{fl/fl}$ mice (Figure S1F). Hence, the RIPK3-GFP fusion protein faithfully reports in vivo expression of RIPK3 without disrupting RIPK3 function.

Real-time PCR analysis using various mouse tissues showed the highest expression of the *Ripk3* transcript in the spleen (Figure S2A), suggesting that RIPK3 is highly expressed in immune cells. Indeed, strong GFP fluorescence signal was detected in various immune cells in the spleen (Figure 1B; Figure S2B). In particular, splenic $CD11c^{-}CD11b^{high}F4/80^{low}$ monocytes expressed RIPK3 at the highest level (Swirski et al., 2009) (Figure 1B). In contrast, $CD11c^{+}CD11b^{+}CD103^{-}$ MNPs, but not $CD11c^{-}CD11b^{+}$ macrophages, showed the highest RIPK3 expression in the colon (Figure 1C; Figure S2C). These results indicate that RIPK3 expression pattern in immune cells is highly variable in different cell types and tissues.

We next examined how inflammation might affect RIPK3 expression. To this end, we first injected lipopolysacharride (LPS) intraperitoneally and analyzed splenocytes for RIPK3 expression. Whereas RIPK3 expression in $CD11c^{-}CD11b^{high}F4/80^{low}$ monocytes was further enhanced (Figure 1D), no significant change in GFP fluorescence was observed in other cell types (Figure S2D). Moreover, RIPK3 protein expression in multiple tissues was unchanged despite clear induction of mature IL-1β (Figure S2E). We previously showed that RIPK3 expression was increased in immune cells in the lamina propria of dextran sodium sulfate (DSS)-treated mice (Moriwaki et al., 2014). Consistent with our previous results, RIPK3-GFP expression in colonic $CD3^{+}$ T cells, but not other immune cells, was significantly increased upon DSS treatment (Figure 1E). In addition, higher RIPK3 expression was found in splenic $CD44^{hi}$ effector-memory T cells compared with $CD44^{lo}$ naive T cells (Figure 1F). In vitro activation of T cells by anti-CD3 and anti-CD28 antibodies or concanavalin A (Con A) also enhanced RIPK3 expression (Figures 1G and S2F). These results indicate that RIPK3 expression is highly inducible in T cells.

The RIPK3 RHIM Is Critical for RIPK3-Mediated Cell Death

RIPK3 has two distinct functional domains: the kinase domain and the RHIM. Studies in knock-in mice expressing kinase inactive RIPK3 ($Ripk3^{K51A/K51A}$ and $Ripk3^{D161N/D161N}$) showed that RIPK3 kinase activity is crucial for necroptosis (Mandal et al., 2014; Newton et al., 2014). In contrast, the physiological function of the RHIM has not been fully explored. To examine the physiological importance of the RHIM, we generated mice specifically lacking RIPK3 RHIM at the C terminus using Cre-loxP-mediated recombination (Figure S3A). We crossed the $Ripk3\text{-}gfp^{fl/fl}$ reporter mice with Sox2-Cre deletor mice to generate mice with germline deletion of the RHIM ($Ripk3^{\Delta R/\Delta R}$) (Figure S3B). Loss of GFP fluorescence signal from all immune cell subsets from $Ripk3^{\Delta R/\Delta R}$ mice was confirmed by flow cytometry (Figure 2A). Because the stop codon of the *Ripk3* gene was removed in the $Ripk3^{\Delta R}$ allele, we performed 3′-rapid amplification of cDNA ends (RACE) experiment using total RNA from $Ripk3^{\Delta R/\Delta R}$ MEFs to determine the C-terminal amino acid sequence of the RIPK3-ΔRHIM protein. The result revealed two possible mRNA transcripts generated from the $Ripk3^{\Delta R}$ allele (Figure S3C). DNA sequencing confirmed that both transcripts are expected to encode truncated and shorter RIPK3 that lack the RHIM (Figure S3D). A widely used rabbit polyclonal antibody that recognizes the C-terminal end of mouse RIPK3 revealed loss of full-length RIPK3 expression from $Ripk3^{\Delta R/\Delta R}$ cells and tissues (Figures 2B and 2C; Figure S3E, middle, RIPK3-P). In contrast, the anti-RIPK3 antibody clone 1G6.1.4 (RIPK3-G) recognized both wild-type RIPK3 and the RIPK3-ΔRHIM proteins that were absent in $Ripk3^{-/-}$ cells (Figures 2B and 2C; Figure S3E, top, RIPK3-G) (Newton et al., 2014). It should be noted that the RIPK3-G antibody detected two bands, both of which were specific for RIPK3 (Newton et al., 2014), and that a single band of RIPK3-ΔRHIM protein was detected between these two wild-type (WT) bands (Figures 2B and 2C). This suggests that WT RIPK3 has two isoforms with different C-terminal sequences. Similar to mice expressing kinase inactive RIPK3 (Mandal et al., 2014), RIPK3-ΔRHIM was expressed at a lower level compared with wild-type RIPK3 (Figures 2B and 2C, top). This suggests that the RHIM and kinase activity are both required to stabilize RIPK3 protein expression.

To evaluate the impact of the RHIM on necroptosis, we treated $Ripk3^{\Delta R/\Delta R}$ MEFs with TNF, the pan-caspase inhibitor zVAD-fmk (zVAD), and cycloheximide (CHX). In contrast with wild-type MEFs, $Ripk3^{\Delta R/\Delta R}$ MEFs were resistant to TNF-induced necroptosis (Figure 2D). $Ripk3^{\Delta R/\Delta R}$ BMDCs were also resistant to necroptosis induced by LPS and zVAD-fmk (Figure 2E) and zVAD-fmk and the Smac mimetic BV6 (Figure 2F), which induces autocrine TNF production (McComb et al., 2012). In addition, $Ripk3^{\Delta R/\Delta R}$ BMDMs were resistant to necroptosis induced by TNF, LPS, or polyinosinic-polycytidylic acid (polyIC) in the presence of the pan-caspase inhibitor zVAD-fmk (Figure 2G). Similar resistance to necroptosis was observed in $Ripk3^{-/-}$ 3T3 cells reconstituted with HA-tagged RIPK3-ΔRHIM proteins (Figure S3F). By contrast, $Ripk3^{\Delta R/\Delta R}$ BMDMs were equally sensitive to apoptosis induced by TNF, LPS, or poly(I:C) (Figure S3G). Moreover, $Ripk3^{\Delta R/\Delta R}$ MEFs were resistant to apoptosis induced by the RIPK3 kinase inhibitor GSK'843 (Figure S3H), which causes caspase-8 activation through RHIM-mediated formation of the ripoptosome (Mandal et al., 2014; Moriwaki and Chan, 2016). Furthermore, $Ripk3^{\Delta R/\Delta R}$ BMDCs were resistant to LPS- and CHX-induced caspase-3/8 activation and apoptosis (Figures S3I and S3J) (Moriwaki et al., 2015). These results indicate that the RIPK3 RHIM is crucial for RIPK3-mediated necroptosis and apoptosis.

$Caspase\text{-}8^{-/-}$ and $Fadd^{-/-}$ mice suffer from embryonic lethality caused by excessive necroptosis. This defect was completely rescued by inactivation of RIPK3 (Kaiser et al., 2011; Oberst et al., 2011). We set up intercrosses of $Fadd^{+/-}Ripk3^{\Delta R/\Delta R}$ mice and found that $Fadd^{-/-}Ripk3^{\Delta R/\Delta R}$ mice were born at a Mendelian ratio (Figure 2H). Moreover, $Fadd^{-/-}Ripk3^{\Delta R/\Delta R}$ mice developed splenomegaly and lymphadenopathy (Figure 2I), and exhibited an expansion of $CD3^{+}B220^{+}CD4^{-}CD8^{-}$ T cells in the spleen (Figure 2J). These phenotypes are characteristic of *lpr* and *gld* mice and the human autoimmune lymphoproliferative syndrome (ALPS) (Lenardo et al., 1999). Hence, the RIPK3 RHIM is essential for necroptosis induced by various physiological stimuli, and deletion of the RHIM is functionally equivalent to the *Ripk3* null allele.

The RHIM Is Essential for RIPK3-Dependent Cytokine Production

We previously reported that RIPK3 promotes NF-κB and inflammasome activation in BMDCs, and that these necroptosis-independent signaling functions are crucial for cytokine production

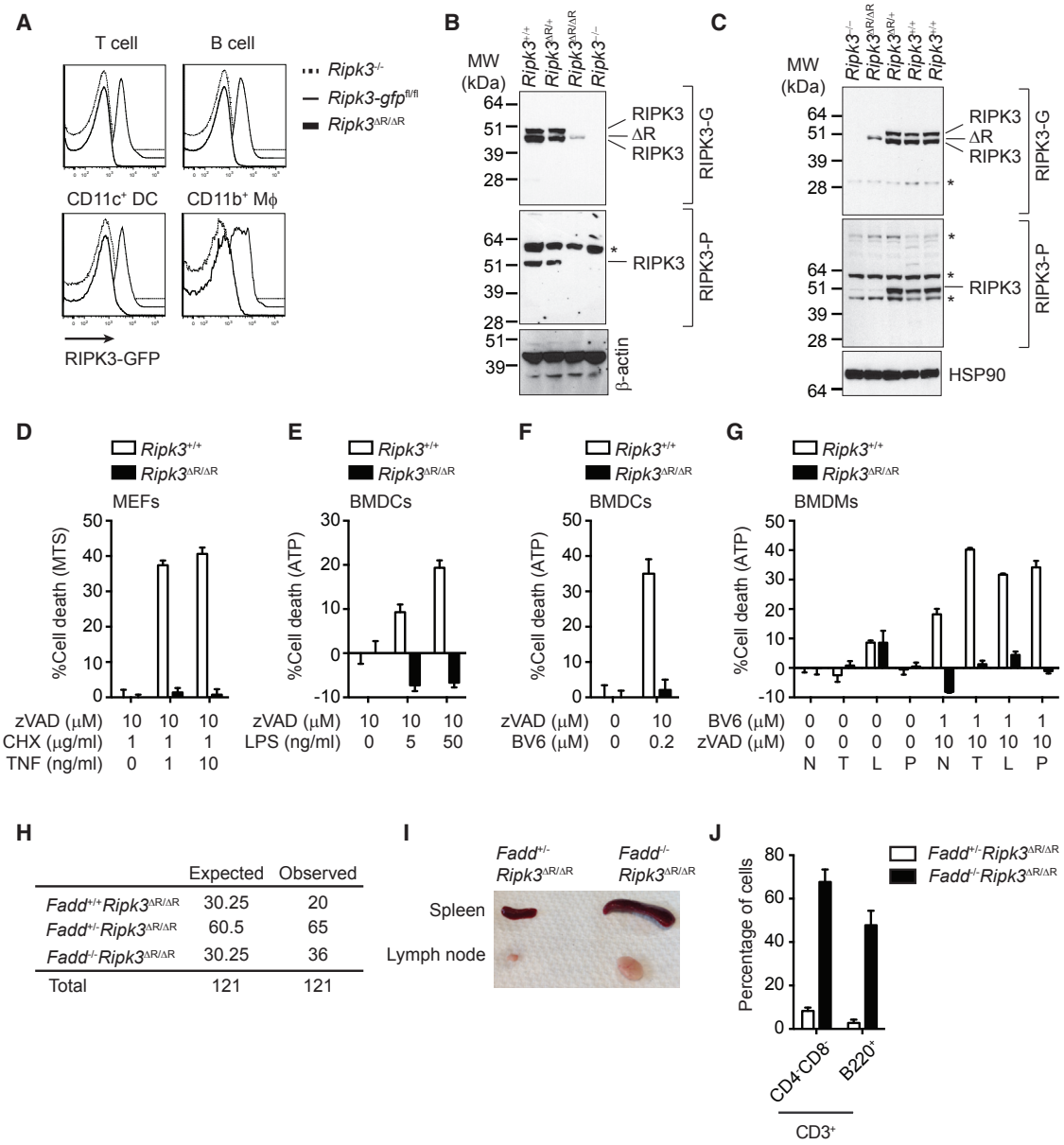

Figure 2. The RIPK3 RHIM Is Essential for Necroptosis

(A) Representative histograms of the GFP fluorescence in splenocytes of mice with indicated genotype are shown.

(B and C) Western blotting of (B) BMDCs and (C) Con A-activated T cell blasts from mice of the indicated genotypes was performed using two distinct anti-RIPK3 antibodies, RIPK3-P and RIPK3-G. The wild-type RIPK3 and RIPK3-ΔRHIM bands are indicated. Asterisks (*) indicate non-specific signals.

(D–G) Necroptosis was induced by various stimuli in (D) MEFs, (E and F) BMDCs, and (G) BMDMs from *Ripk3*$^{+/+}$ and *Ripk3*$^{\Delta R/\Delta R}$ mice. L, 100 ng/mL LPS; N, no stimulation; P, 20 μg/mL poly(I:C); T, 100 ng/mL TNF.

(H) *Fadd*$^{+/-}$*Ripk3*$^{\Delta R/\Delta R}$ mice were intercrossed, and the number of offspring with each genotype is shown.

(I) A representative picture of the spleen and lymph node in 13-week-old mice of the indicated genotypes is shown.

(J) Splenocytes from 13-week-old mice of the indicated genotypes were analyzed by flow cytometer.

Results shown are mean ± SEM of triplicates. See also Figure S3.

downstream of TLR4 (Moriwaki et al., 2014). In contrast with BMDCs treated with an RIPK3 kinase inhibitor (Moriwaki et al., 2014), LPS-induced *Il23p19* expression was reduced in *Ripk3*$^{\Delta R/\Delta R}$ BMDCs (Figure 3A). TNF expression was also significantly diminished in LPS-treated *Ripk3*$^{\Delta R/\Delta R}$ BMDCs (Figure 3B). The RelB-p50 heterodimer potently induces *Il23p19* expression by BMDCs in response to TLR stimulation (Shih et al., 2012). This led us to test whether the RIPK3 RHIM is required for optimal RelB-p50 activation and cytokine expression (Moriwaki et al., 2014). Indeed, LPS-induced nuclear translocation of

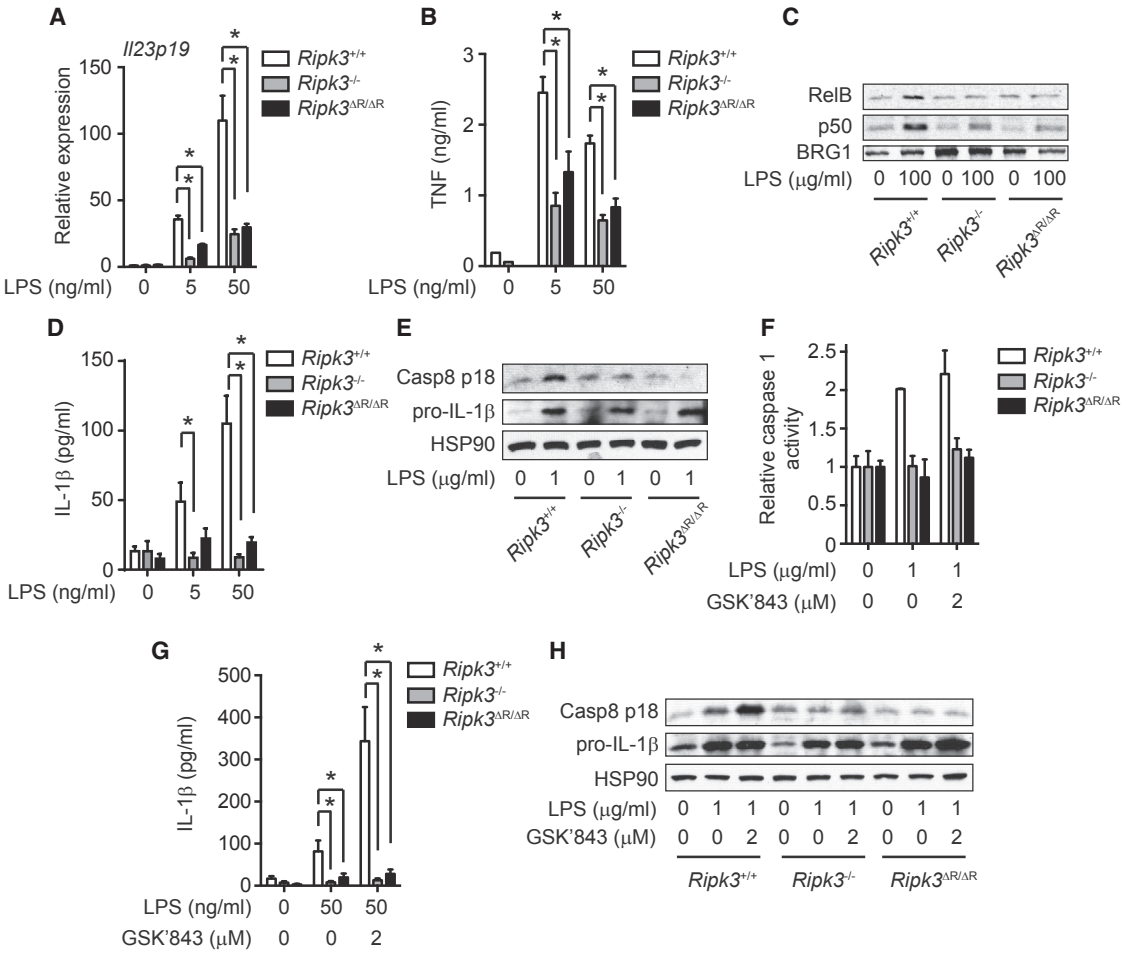

Figure 3. The RIPK3 RHIM Is Required for Cytokine Production in BMDCs

(A–H) *Ripk3*$^{+/+}$, *Ripk3*$^{-/-}$, and *Ripk3*$^{\Delta R/\Delta R}$ BMDCs were stimulated with LPS for 6 hr (A, B, D, and G), 2 hr (C), or 1 hr (E, F, and H). (F–H) Where indicated, the cells were pretreated with GSK'843 for 1 hr. (A) *Il23p19* expression was determined by Q-PCR (n = 3). (B, D, and G) TNF (B) and IL-1β (D and G) secretion were determined by ELISA (n = 3–8). (F) Caspase-1 activity was quantified using fluorescent substrate YVAD-AFC (n = 2). (C, E, and H) Nuclear extracts (C) or whole-cell lysates (E and H) were subjected to western blotting. Results shown are mean ± SEM. *p < 0.05.

RelB and p50 was similarly impaired in *Ripk3*$^{\Delta R/\Delta R}$ and *Ripk3*$^{-/-}$ BMDCs (Figure 3C).

In monocytes and DCs, LPS alone is sufficient to stimulate mature IL-1β secretion without a second inflammasome activation signal (He et al., 2013; Moriwaki et al., 2015). This response requires an intact RIPK3, but not its kinase activity (Moriwaki et al., 2015). LPS-induced IL-1β secretion was blunted in *Ripk3*$^{\Delta R/\Delta R}$ BMDCs (Figure 3D), indicating that unlike the kinase activity, the RHIM is essential for this function. Mature IL-1β secretion is achieved by cleavage of pro-IL-1β by caspase-1 or caspase-8 (Latz et al., 2013). The activation of both caspases was equally impaired in *Ripk3*$^{\Delta R/\Delta R}$ and *Ripk3*$^{-/-}$ BMDCs (Figures 3E and 3F). RIPK3 stimulates caspase-8-mediated cleavage of pro-IL-1β through a ripoptosome-like complex (Kang et al., 2015; Lawlor et al., 2015; Moriwaki et al., 2015). Assembly of this complex is enhanced by addition of GSK'843, which causes a conformational change of RIPK3 to promote interaction with RIPK1, FADD, and caspase-8 (Moriwaki et al., 2015). GSK'843 enhanced LPS-induced caspase-8 activation and IL-1β secretion in *Ripk3*$^{+/+}$ BMDCs (Figures 3G and 3H). In contrast, GSK'843 failed to stimulate IL-1β secretion or caspase-8 activation in *Ripk3*$^{\Delta R/\Delta R}$ BMDCs (Figures 3G and 3H). Hence, unlike its kinase activity, the RIPK3 RHIM is essential for optimal LPS-induced NF-κB and inflammasome activation.

The RHIM of RIPK3 Mediates Protection against DSS-Induced Colitis

DSS induces intestinal epithelial cell injury, and the resultant inflammation exhibits certain features resembling acute colitis. We previously showed that RIPK3-mediated expression of the cytokines IL-23, IL-1β, and IL-22 has a crucial role in the resolution of intestinal injury (Moriwaki et al., 2014). To determine whether this tissue repair function of RIPK3 requires an intact RHIM, we treated *Ripk3*$^{\Delta R/\Delta R}$ mice with DSS for 7 days, followed by recovery in normal drinking water for another 7 days. When compared with *Ripk3*$^{+/+}$ littermates, *Ripk3*$^{\Delta R/\Delta R}$ mice suffered

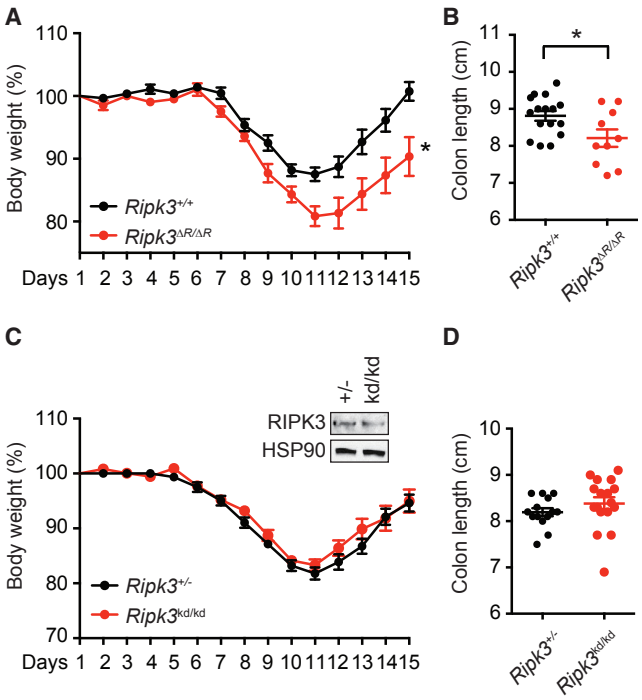

Figure 4. The RIPK3 RHIM, but Not Its Kinase Activity, Mediates Protection against DSS

(A–D) *Ripk3*$^{\Delta R/\Delta R}$ (n = 10) and *Ripk3*$^{+/+}$ littermates (n = 16) (A and B), or *Ripk3*$^{kd/kd}$ (n = 17) and *Ripk3*$^{+/-}$ co-housed mice (n = 14) (C and D) were treated with 3% DSS for 7 days, followed by regular water for an additional 7 days. (A and C) Body weight was measured daily. (B and D) Colon length was measured on day 15. The inset in (C) shows equal RIPK3 protein expression between *Ripk3*$^{kd/kd}$ and *Ripk3*$^{+/-}$ colon. Results shown are mean ± SEM. *p < 0.05.

from more severe body weight loss (Figure 4A). In addition, colon length after DSS treatment was significantly reduced in *Ripk3*$^{\Delta R/\Delta R}$ mice (Figure 4B). In contrast, *Ripk3*$^{kd/kd}$ (K51A) kinase inactive mice developed similar intestinal inflammation compared with co-housed *Ripk3*$^{+/-}$ controls, in which RIPK3 protein is expressed at the level similar to RIPK3 K51A protein, as determined by body weight loss and colon length on day 15 (Figures 4C and 4D). Because the kinase activity of RIPK3 is essential for necroptosis, these results indicate that RIPK3 mediates reparative inflammation in the intestine through RHIM-dependent, but necroptosis- and kinase-independent, mechanisms.

RIPK3 Promotes Injury-Induced Cytokine Expression by CD11c$^+$ Cells

Radiation BM chimera experiments revealed that RIPK3 expression in hematopoietic cells was important for protection against DSS-induced colitis (Moriwaki et al., 2014). Adoptive transfer of LPS-treated *Ripk3*$^{+/+}$ BMDCs, but not *Ripk3*$^{-/-}$ BMDCs, rescued production of the tissue-repair-associated cytokines IL-22, IL-23, and IL-1β. Because RIPK3 promotes optimal cytokine expression in BMDCs, we reasoned that DC-like cells are responsible for the protective effect of RIPK3 in DSS-induced colitis and tissue repair. To test our hypothesis, we generated DC-specific *Ripk3*$^{\Delta R/\Delta R}$ (*CD11c:Ripk3-gfp*$^{fl/fl}$) mice by crossing the *Ripk3-gfp*$^{fl/fl}$ reporter mice with CD11c (*Itgax*)-Cre transgenic mice. Flow cytometry confirmed that the GFP fluorescence signal was lost in CD11c$^+$ cells (Figure 5A). Consistent with the reported weak activity of the CD11c-Cre transgene in T and B cells (Caton et al., 2007), we also observed slight reduction in GFP signals in these cells. When the *CD11c:Ripk3-gfp*$^{fl/fl}$ mice were challenged with DSS, they exhibited much more severe body weight loss and shortening of the colon than *Ripk3-gfp*$^{fl/fl}$ littermates (Figures 5B and 5C). Similar to *Ripk3*$^{-/-}$ mice (Moriwaki et al., 2014), *CD11c:Ripk3-gfp*$^{fl/fl}$ mice produced significantly reduced IL-22, a critical promoter of tissue repair, in the colon after DSS treatment than littermate controls (Figure 5D). In addition, expression of IL-23 and IL-1β, which stimulate IL-22 production by type 3 innate lymphoid cells (Lee et al., 2013), was also significantly suppressed in the colon of DSS-treated *CD11c:Ripk3-gfp*$^{fl/fl}$ mice (Figure 5D). By contrast, TNF expression, which was normal in DSS-treated *Ripk3*$^{-/-}$ mice (Moriwaki et al., 2014), was also unaffected in *CD11c:Ripk3-gfp*$^{fl/fl}$ mice (Figure S4A). The number of T cells, B cells, and CD11c$^+$ and CD11b$^+$ MNPs in the intestinal lamina propria was similar in *Ripk3-gfp*$^{fl/fl}$ and *CD11c:Ripk3-gfp*$^{fl/fl}$ mice (Figures S4B and S4C). In addition, the percentage of type 3 innate lymphoid cells and RIPK3 in these cells was also unchanged in *CD11c:Ripk3-gfp*$^{fl/fl}$ mice (Figures S4D and S4E). These results are consistent with those observed in germline *Ripk3*$^{-/-}$ mice and indicate that RIPK3 promotes optimal expression of repair-associated cytokines by CD11c$^+$ cells in a cell-intrinsic manner.

The Role of Colonic CX$_3$CR1$^+$ MNPs in RIPK3-Dependent Cytokine Expression

Colonic CD11c$^+$ cells are subdivided into two main populations: CD11c$^+$CD11b$^+$CD103$^-$ and CD11c$^+$CD11b$^-$CD103$^+$ cells (Figure S2C) (Denning et al., 2011). Whereas CD11c$^+$CD11b$^-$CD103$^+$ cells are considered to be conventional DCs developed from common DC precursors, CD11c$^+$CD11b$^+$CD103$^-$ cells are developed from monocytes and express both DC and macrophage markers (Cerovic et al., 2014). Within the CD11c$^+$CD11b$^+$CD103$^-$ MNPs, the chemokine receptor CX$_3$CR1 was reported to mark a population of cells that are the main source of IL-23 and IL-1β during intestinal inflammation (Longman et al., 2014). We therefore tested the role of RIPK3 in cytokine production by the CX$_3$CR1$^+$ MNPs. Because no reliable CX$_3$CR1 antibody is available for flow cytometry, we used CD14 as a marker to test RIPK3 expression in this population. Consistent with a previous report (Diehl et al., 2013), we confirmed by using *Cx$_3$cr1*$^{gfp/+}$ reporter mice that the CD11c$^+$MHC-II$^+$CD14$^+$ MNPs were indeed exclusively positive for CX$_3$CR1 expression (Figure S5A). Interestingly, these CD11c$^+$CD11b$^+$CD103$^-$CD14$^+$ MNPs also expressed high levels of RIPK3 compared with CD11c$^+$CD11b$^-$CD103$^+$ DCs (Figure 6A). We isolated CX$_3$CR1$^+$ MNPs and CD103$^+$ DCs from colonic lamina propria of untreated *Ripk3*$^{+/+}$*Cx3cr1*$^{gfp/+}$ and *Ripk3*$^{-/-}$*Cx3cr1*$^{gfp/+}$ mice or the mice challenged with DSS for 7 days and compared their cytokine expression profile (Figure S5B). Consistent with a published report (Longman et al., 2014), *Il23p19* and *Il1b* expression were induced in CX$_3$CR1$^+$ MNPs in response to DSS (Figure 6B). In contrast, the cytokine expression was undetectable in CD103$^+$

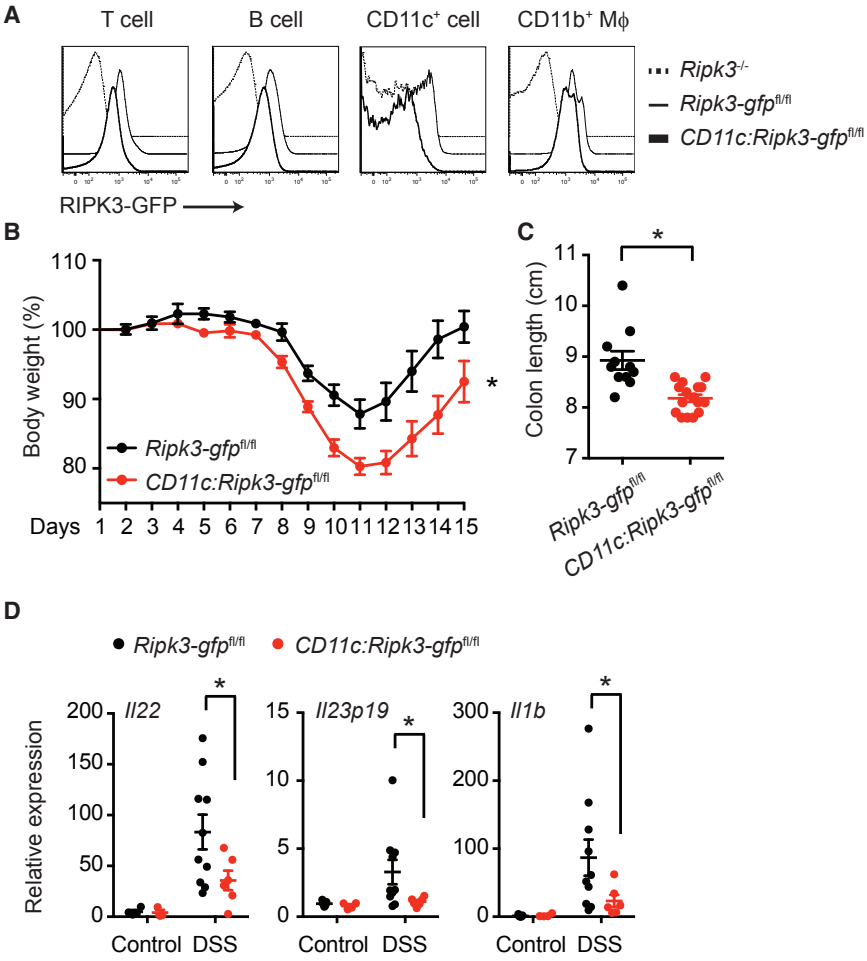

Figure 5. CD11c$^+$ Cell-Specific Deletion of the RIPK3 RHIM Confers Protection against DSS

(A) Representative histograms of the GFP fluorescence intensity in colonic lamina propria mononuclear cells from mice of the indicated genotypes are shown.

(B and C) *Ripk3-gfp*$^{fl/fl}$ (n = 11) and *CD11c:Ripk3-gfp*$^{fl/fl}$ littermates (n = 16) were treated with 3% DSS for 7 days, followed by regular water for an additional 7 days. Body weight was measured daily (B). Colon length on day 15 is shown (C).

(D) Expression of *Il22*, *Il23p19*, and *Il1b* in colon from the mice treated with DSS for 7 days was determined by qPCR (n = 3–10).

Results shown are mean ± SEM. *p < 0.05. See also Figure S4.

DCs (Figure 6B). Strikingly, the expression of *Il23p19* was significantly reduced in CX_3CR1^+ MNPs isolated from *Ripk3*$^{-/-}$ *Cx3cr1*$^{gfp/+}$ mice compared with those from *Ripk3*$^{+/+}$*Cx3cr1*$^{gfp/+}$ littermates. The expression of *Il1b* was also reduced in CX_3CR1^+ MNPs isolated from *Ripk3*$^{-/-}$*Cx3cr1*$^{gfp/+}$ mice, although the difference was not statistically significant. To determine whether CX_3CR1^+ MNPs are responsible for the impaired cytokine expression in *CD11c:Ripk3-gfp*$^{fl/fl}$ mice, we isolated CD11c$^+$ CD11b$^+$CD14$^+$ MNPs from DSS-treated *Ripk3-gfp*$^{fl/fl}$ and *CD11c:Ripk3-gfp*$^{fl/fl}$ mice. Indeed, the cells from *CD11c:Ripk3-gfp*$^{fl/fl}$ mice also exhibited reduction in *Il1b* and *Il23p19* expression (Figure S5C), although the difference was not statistically significant. Collectively, these results suggest that CX_3CR1^+ MNPs in the lamina propria contribute to injury-induced cytokine expression.

DISCUSSION

RIPK3 is a key signal adaptor for necroptosis. Recently, RIPK3 has also been shown to promote activation of the NLRP3 inflammasome, NF-κB, and apoptosis. The role of RIPK3 in necroptosis-independent signaling is especially prominent in innate immune sentinels such as macrophages and DCs. However, tools that allow examination of RIPK3 functions in distinct cell populations have been lacking. In this study, we report two mouse models that address this deficiency. Using the RIPK3-GFP reporter mice, we found that RIPK3 expression is dynamically regulated in different immune subsets. For example, RIPK3 expression was increased in macrophages in response to LPS stimulation. In contrast, RIPK3 expression was strongly induced in T cells during intestinal inflammation. T-cell-receptor-dependent induction of RIPK3 expression suggests that RIPK3 may regulate T cell responses and functions. Indeed, previous studies showed that *Fadd*$^{-/-}$*Ripk3*$^{-/-}$ and *Casp8*$^{-/-}$*Ripk3*$^{-/-}$ mice developed an *lpr/gld*-like autoimmune disease (Dillon et al., 2012; Kaiser et al., 2011; Oberst et al., 2011), indicating that RIPK3 cooperates with FADD/caspase-8 to enforce peripheral T cell tolerance. Whether RIPK3 regulates other functions in T cells is unknown at present.

In contrast with T cells, RIPK3 has a key role in cytokine expression by DCs and macrophages. RIPK3 expression in CD11c$^+$ DCs and CD11b$^+$ macrophages was not dramatically altered during LPS- or DSS-induced inflammation, although its expression in these innate immune effectors in different anatomical locations is highly variable. For instance, CD11c$^+$MHC-II$^+$CD11b$^+$ MNPs in the colonic lamina propria highly expressed RIPK3 compared with those in spleen and showed the highest RIPK3 expression among various immune cell subsets. These cells have been implicated to be major producers of IL-23 and IL-1β, which in turn stimulate IL-22 production by type 3 innate lymphoid cells (Aychek et al., 2015; Longman et al., 2014; Manta et al., 2013). Depletion of this population or knockout of CX_3CR1 exacerbated experimental colitis (Longman et al., 2014; Medina-Contreras et al., 2011). Although some of the effect might be because of the reduced expression of RIPK3-ΔRHIM protein, deletion of the RIPK3 RHIM in CD11c$^+$ cells alone was sufficient to recapitulate the severe colitis observed in germline *Ripk3*$^{-/-}$ mice. This observation strongly suggests that the RHIM is

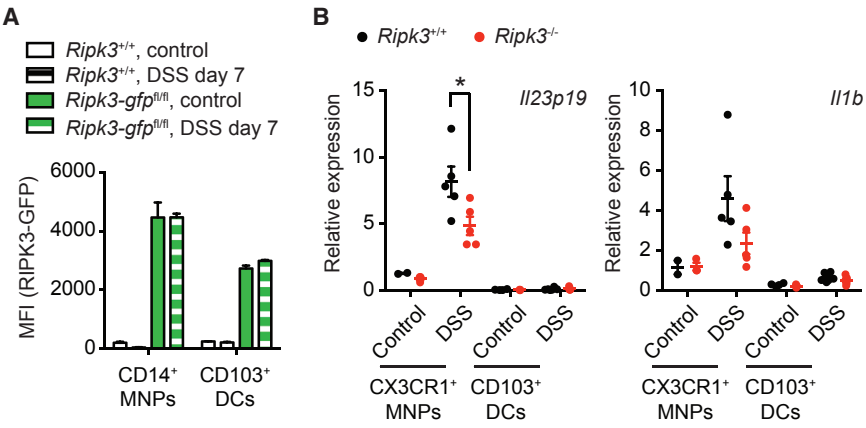

Figure 6. RIPK3 Promotes Cytokine Production by Colonic CX_3CR1^+ MNPs

(A) Mononuclear cells from untreated or DSS-treated *Ripk3-gfp*$^{fl/fl}$ and *Ripk3*$^{+/+}$ mice were analyzed for RIPK3-GFP mean fluorescence intensity (MFI). $CD14^+$ MNPs and $CD103^+$ DCs were defined as $CD45^+CD3^-CD19^-CD11c^+MHC\text{-}II^+CD14^+CD103^-$ (for $CD14^+$ MNPs) and $CD45^+CD3^-CD19^-CD11c^+MHC\text{-}II^+CD14^-CD103^+$ (for $CD103^+$ DCs), respectively (n = 5–6).

(B) $CD45^+CD11c^+MHC\text{-}II^+CD11b^+CX_3CR1^+$ MNPs and $CD45^+CD11c^+MHC\text{-}II^+CD11b^-CD103^+$ DCs were FACS-sorted from mice treated with DSS for 7 days and subjected to RNA extraction and qPCR analysis (n = 2–6).

Results shown are mean ± SEM. *p < 0.05. See also Figure S5.

essential for necroptosis-dependent and -independent functions of RIPK3. *Ripk3*$^{-/-}$ CX_3CR1^+ MNPs and CX_3CR1^+ MNPs from *CD11c:Ripk3-gfp*$^{fl/fl}$ mice produced reduced levels of *Il-1b*, *Il23p19*, and *Il22*, although the differences were not always statistically significant. Thus, there may be other immune effectors within the lamina propria that require RIPK3 to achieve optimal cytokine expression.

RIPK3 is widely believed to induce inflammation through necroptosis-associated release of damage-associated molecular patterns (Kaczmarek et al., 2013). This current dogma is mostly based on studies from mice lacking caspase-8 or FADD, or multiple cellular inhibitor of apoptosis proteins (cIAPs), all of which are strong inhibitors of RIPK3 pro-necroptotic function (Chan et al., 2015). It is therefore striking that unlike *Ripk3*$^{\Delta R/\Delta R}$ or *Cd11c-Cre:Ripk3-gfp*$^{fl/fl}$ mice, *Ripk3*$^{kd/kd}$ mice did not develop more severe colitis. Thus, in injury-induced cytokine expression and tissue repair, RIPK3 functions exclusively as an inducer of cytokine expression rather than as a cell death adaptor. A necroptosis-independent role for RIPK3 in NLRP3 inflammasome activation has been observed in in vitro studies with BMDMs and BMDCs (Kang et al., 2015; Lawlor et al., 2015; Moriwaki et al., 2015; Vince et al., 2012). However, as in the case of necroptosis, maximal RIPK3-mediated inflammasome activation also requires FADD, caspase-8, or cIAPs inhibition. Thus, our result demonstrates a necroptosis-independent role for RIPK3 in physiological inflammation without pharmacological or genetic manipulation of FADD, caspase-8, or cIAPs. Our results also reveal that the non-necroptotic functions of RIPK3 may be confined to specific cell compartments. In this scenario, its function can only be revealed using tissue-specific inactivation approaches.

We previously reported that the RIPK3-RIPK1-FADD-caspase-8 complex was formed upon LPS stimulation in BMDCs. Assembly of this ripoptosome-like complex also requires another RHIM-containing adaptor TRIF (Moriwaki et al., 2015). Results from this present study indicate that an intact RHIM is not only crucial for necroptosis, but also for RIPK3-dependent ripoptosome assembly and pro-IL-1β processing. However, this function of RIPK3 does not require its pro-necroptotic kinase activity. In contrast, the mechanism by which RIPK3 promotes RelB-p50 activation is less understood. RIPK3 has been implicated to shuttle between the cytoplasm and nucleus (Yang et al., 2004; Yoon et al., 2016), suggesting that RIPK3 may directly engage the transcriptional machinery under certain conditions.

EXPERIMENTAL PROCEDURES

Mice

To generate *Ripk3-gfp*$^{fl/fl}$ reporter mice, we created a targeting construct in which an *eGfp* sequence was inserted at the end of the coding region of the *Ripk3* gene. The neomycin resistance gene flanked by flippase recognition target (FRT) sites was inserted in intron 9 for positive selection. For negative selection, thymidine kinase was added outside the 5′ homology arm. LoxP sites were also inserted before the neomycin cassette and after the EGFP sequence. Embryonic stem (ES) cells were transfected with the targeting construct and subsequently selected by neomycin in the transgenic animal core at the University of Massachusetts Medical School (UMMS). ES clones in which proper recombination occurs were selected by Southern blot analysis, with probe 1 located in the 5′ homology arm and probe 2 located outside the 3′ homology arm and subsequently used for injection into albino C57BL/6 blastocysts to generate chimeric mice. Germline transmission of the transgene was confirmed by Southern blot analysis. The neomycin cassette was removed by crossing the *Ripk3-gfp*$^{flox\text{-}neo/+}$ mice with the flippase transgenic mice [Gt(ROSA)26Sor$^{tm1(Flp1)Dym}$, kindly provided from S. Jones in UMMS]. To generate mice constitutively deficient for the *Ripk3* RHIM, we crossed *Ripk3-gfp*$^{flox\text{-}neo/+}$ mice with Sox2-Cre transgenic mice (kindly provided from S. Jones in UMMS). The resultant *Ripk3*$^{fl/+}$ and *Ripk3*$^{\Delta RHIM/+}$ mice were backcrossed with C57BL/6 mice for 8–10 generations. To delete the RHIM specifically in $CD11c^+$ cells, we crossed *Ripk3-gfp*$^{fl/fl}$ mice with CD11c (Itgax)-Cre transgenic mice obtained from The Jackson Laboratory. *Ripk3*$^{-/-}$ mice were obtained from Genentech. *Fadd*$^{-/-}$ mice were described before (Zhang et al., 2011). *Ripk3* K51A kinase dead knock-in (*Ripk3*$^{kd/kd}$) mice were generated in GlaxoSmithKline (Mandal et al., 2014). *Cx3cr1*$^{gfp/gfp}$ reporter mice were obtained from The Jackson Laboratory. All animal experiments were approved by the institutional animal care and use committee. The RIP3-GFP floxed mice are available at The Jackson Laboratory as Stock No. 030284.

DSS Treatment

Female mice (9–12 weeks old) were treated with 3% DSS (molecular mass 36,000–50,000 Da; MP Biomedicals) for 7 days. The DSS water was replaced with fresh DSS water on days 3 and 5 and with regular water on day 8. Body weight was monitored for 15 days, and the weight at the beginning of the experiments was normalized as 100%. To obtain *Ripk3*$^{+/-}$ control mice with a minimum difference of genetic background, we crossed *Ripk3*$^{kd/+}$ mice with *Ripk3*$^{-/-}$ mice. The resultant *Ripk3*$^{kd/-}$ or *Ripk3*$^{+/-}$ mice were intercrossed to obtain *Ripk3*$^{kd/kd}$ or *Ripk3*$^{+/-}$ mice. After weaning, these mice were co-housed

to minimize the influence of intestinal microflora. All experiments, except for the ones using *Ripk3*$^{kd/kd}$ mice, were performed using littermates. To minimize the differences in intestinal microbial environment among cages, we mixed bedding materials from different cages once a week after weaning.

Flow Cytometry

Colon was harvested from untreated or DSS-treated mice. After removing feces with PBS, the colon was longitudinally opened and cut into three pieces. The tissues were washed with PBS and subsequently incubated in 1 mM DTT for 10 min at room temperature (RT). Then, the tissues were shaken in 10 mM HEPES buffer containing 30 mM EDTA for 10 min at 37°C (225 rpm). After washing, the tissues were digested with 0.5 mg/mL collagenase IV (Sigma) and 150 μg/mL DNase I (Sigma) for 90 min at 37°C. Tissues were broken by vigorously shaking, filtered, and subjected to Percoll density gradient separation. LPMCs at the interphase of the two Percoll solutions were collected and subjected to flow cytometric analysis. To isolate splenocytes, we incubated spleen with 2 mg/mL collagenase D solution (10 mM HEPES [pH 7.4], 150 mM NaCl, 5 mM KCl, 1 mM $MgCl_2$, 1.8 mM $CaCl_2$) for 30 min at 37°C. After gliding the spleen, red blood cells were lysed with ACK lysis buffer (150 mM NH_4Cl, 10 mM $KHCO_3$, 0.1 mM EDTA). Splenocytes were filtered and subjected to flow cytometric analysis. Prior to incubation with primary antibodies, cells were incubated with anti-Fc receptor 2.4G2 antibody for 10 min. PE-labeled anti-CD3 (145-2C11), PerCP-Cy5.5-labeled anti-CD11b (M1/70), Pacific blue-labeled anti-F4/80 (BM8), Pacific blue-labeled anti-CD45.2 (104), biotin-labeled CD103 (2E7), PerCP-Cy5.5-labeled anti-CD8b (YTS/56.7.7), and PE-labeled anti-MHCII I-A^b (AF6-120.1) antibodies were obtained from BioLegend. PE-Cy7-labeled CD19 (eBio10-3), PE-Cy7-labeled CD44 (IM7), PE-Cy7-labeled anti-CD14 (Sa2-8) antibodies, and allophycocyanin (APC)-eFluor780-labeled streptavidin were obtained from eBioscience. APC-labeled anti-CD11c (HL3), APC-Cy7-labeled anti-CD8a (53-6.7), APC-labeled anti-CD3 (145-2C11), APC-Cy7-labeled anti-CD4 (GK1.5), FITC-labeled anti-CD19 (1D3), PE-labeled anti-B220 (RA3-6B2), Alexa Fluor 647-labeled CCR6 (140706), PE-labeled Ter119 (TER-119), and Pacific blue-labeled anti-CD4 (RM4-5) antibodies were obtained from BD Biosciences. Cells were analyzed by LSRII (BD Biosciences). For cell sorting, FACSAria II (BD Biosciences) was used.

T Cell Stimulation

A 24-well tissue culture plate was coated with 10 μg/mL anti-CD3 (145-2C11) and 5 μg/mL anti-CD28 (37.51) antibodies at 4°C overnight. Splenocytes were plated onto the coated plate. For Con A stimulation, splenocytes were plated onto uncoated plate and stimulated with 5 μg/mL Con A. After 3 days, the cells were subjected to flow cytometric analysis.

Western Blot

Cell lysates prepared using radio-immunoprecipitation assay (RIPA) lysis buffer supplemented with protease (Roche) and phosphatase inhibitors (Sigma) were subjected to SDS-PAGE. Nuclear extracts were prepared as described before (Moriwaki et al., 2014). After transferring proteins to nitrocellulose membrane, immunoblot analysis was performed with the following antibodies: anti-RIPK3 (2283, RIPK3-P; Prosci), anti-mouse RIPK3 (clone 1G6.1.4, RIPK3-G; Genentech), anti-HSP90 (68/Hsp90; BD Biosciences), anti-HA, anti-RelB (C1E4; Cell Signaling), anti-p50 (H-119; Santa Cruz), anti-BRG1 (kindly provided by A. Imbalzano), anti-caspase-8 (1G12; Enzo Lifesciences), anti-pro-IL-1β (AF-401-NA; R&D Systems), and anti-caspase-3 (46; Santa Cruz) antibodies.

Cell Culture and Stimulation

BM cells were cultured for 7 days in either RPMI media supplemented with 10 ng/mL GM-CSF and 5 ng/mL IL-4 to generate BMDCs or L929-conditioned media to generate BMDMs (Moriwaki et al., 2014). *Ripk3*$^{+/+}$, *Ripk3*$^{-/-}$, *Ripk3*$^{\Delta R/\Delta R}$ MEFs, *Ripk3*$^{-/-}$ 3T3, and 293T cells were cultured in DMEM media. Ten percent fetal calf serum, 2 mM glutamine, 100 U/mL penicillin, and 100 μg/mL streptomycin were added to the media. Purified LPS from Invivogen was used for all experiments. In some experiments, cells were pretreated with zVAD-fmk (Enzo Lifesciences), CHX (Sigma), BV6 (kindly provided from D. Vucic in Genentech), and/or RIPK3 kinase inhibitor GSK2393843A (GSK'843; GlaxoSmithKline) for an hour prior to LPS, TNF, or polyIC stimulation, unless otherwise stated. After stimulation, culture media and cells were used for cell death assay, ELISA, RNA, and protein analyses. Caspase-1 activity was measured by caspase-1 substrate YVAD-7-amido-4-trifluoromethylcoumarin (YVAD-AFC) (BioVision).

qPCR

Total RNA was extracted from cells and tissues using RNeasy Mini kit (QIAGEN) and subjected to reverse transcription using Superscript III (Invitrogen). Real-time PCR analysis using iQ SYBR Green Supermix (Bio-Rad Laboratories) was performed on C1000 thermal cycler and CFX96 real-time system (Bio-Rad laboratories). The following primers were used: 5′-TTGAGGTGTCCA ACTTCCAGCA-3′ and 5′-AGCCGGACATCTGTGTTGTTA-3′ for *Il22*, 5′-CCAG CGGGACATATGAATCT-3′ and 5′-AGGCTCCCCTTTGAAGATGT-3′ for *Il23a (Il23p19)*, 5′-CCCAACTGGTACATCAGCAC-3′ and 5′-TCTGCTCATTCACGAA AAGG-3′ for *Il1b*, 5′-TGTCAAGTTATGGCCTACTGGTGCG-3′ and 5′-AACCAT AGCCTTCACCTCCCAGGAT-3′ for *Ripk3*, and 5′-CAAACCCAGAATTGTTCT CCTT-3′ and 5′-ATGTGGTCTTCCTGAATCCCT-3′ for *Tbp*.

Cell Death Assay

Cell death was determined by CellTiter-Glo Luminescent Cell Viability Assay (Promega), CytoTox 96 Non-Radioactive Cytotoxicity Assay (Promega), or CellTiter 96 AQ_{ueous} One Solution Cell Proliferation Assay (Promega). All cell death assays were performed in triplicates.

3′-RACE PCR

DNA sequence of the 3′ region of *Ripk3*$^{\Delta R}$ mRNA was determined by 3′-RACE experiment (Scotto-Lavino et al., 2006). Total RNA was extracted from *Ripk3*$^{\Delta R/\Delta R}$ MEFs and reverse transcribed using Q^{total} primer (5′-CCAGTGAG CAGAGTGACGAGGACTCGAGCTCAAGCTTTTTTTTTTTTTTTT-3′) and Superscript III. First PCR was performed using Q^{outer} primer (5′-CCAGTGAGCAG AGTGACG-3′) and gene-specific primer (GSP) 1 (5′-TGCTGCTGTCTCCGAG GTAAAG-3′). PCR product was subjected to second PCR using Q^{inner} primer (5′-ATCGGATCCGAGGACTCGAGCTCAAGC-3′) and GSP2 (5′-ATCGAATTC CAAAGGAATCAGGGAGATGGAAG-3′). Pfu Turbo DNA polymerase AD was used for PCR. PCR product was run on a 1% agarose gel and purified from the gel. The purified products were digested by EcoRI and HindIII, and subsequently cloned into pUC19 vector. DNA sequence was determined by sequence analysis.

Plasmids, Viruses, Transfections, and Transductions

Mouse wild-type *Ripk3* gene and *Ripk3*$^{\Delta R}$ short and long isoforms were cloned into a modified lentiviral tet-on pTRIPZ/Puro vector. HA tag was introduced at the amino terminus of RIPK3 by PCR cloning. The sequence of all the genes inserted was confirmed by sequence analysis. *Ripk3*$^{-/-}$ 3T3 cells were transduced by lentivirus generated in 293T cells with pTRIPZ, pMD2.G, and psPAX2 vectors. After transduction, the cells were selected by 2 μg/mL puromycin.

Statistical Analysis

The p values were calculated using unpaired t test with Welch's correction or two-way repeated-measures ANOVA. The p values <0.05 were considered statistically significant.

SUPPLEMENTAL INFORMATION

Supplemental Information includes five figures and can be found with this article online at http://dx.doi.org/10.1016/j.celrep.2017.02.015.

AUTHOR CONTRIBUTIONS

K.M. and F.K.-M.C. designed the project. K.M. and S.B. performed experiments. J.B. and P.J.G. provided critical reagents. K.M. and F.K.-M.C. wrote the paper. F.K.-M.C. supervised the project.

ACKNOWLEDGMENTS

We thank Stephen Jones (UMMS) for the flippase and Cre deletor mice, Anthony Imbalzano (UMMS) for the anti-BRG1 antibody, Domagoj Vucic

(Genentech) for BV6, and Kim Newton and Vishva Dixit for the RIPK3-G antibody. This work is supported by NIH grant AI119030 (F.K.-M.C.) and a Crohn's & Colitis Foundation of America Senior Research Award (326364 to F.K.-M.C.). J.B. and P.J.G. are employees of GlaxoSmithKline.

Received: April 16, 2016
Revised: December 28, 2016
Accepted: February 1, 2017
Published: March 7, 2017

REFERENCES

Aychek, T., Mildner, A., Yona, S., Kim, K.W., Lampl, N., Reich-Zeliger, S., Boon, L., Yogev, N., Waisman, A., Cua, D.J., and Jung, S. (2015). IL-23-mediated mononuclear phagocyte crosstalk protects mice from Citrobacter rodentium-induced colon immunopathology. Nat. Commun. *6*, 6525.

Cai, Z., Jitkaew, S., Zhao, J., Chiang, H.C., Choksi, S., Liu, J., Ward, Y., Wu, L.G., and Liu, Z.G. (2014). Plasma membrane translocation of trimerized MLKL protein is required for TNF-induced necroptosis. Nat. Cell Biol. *16*, 55–65.

Caton, M.L., Smith-Raska, M.R., and Reizis, B. (2007). Notch-RBP-J signaling controls the homeostasis of CD8- dendritic cells in the spleen. J. Exp. Med. *204*, 1653–1664.

Cerovic, V., Bain, C.C., Mowat, A.M., and Milling, S.W. (2014). Intestinal macrophages and dendritic cells: what's the difference? Trends Immunol. *35*, 270–277.

Chan, F.K., Luz, N.F., and Moriwaki, K. (2015). Programmed necrosis in the cross talk of cell death and inflammation. Annu. Rev. Immunol. *33*, 79–106.

Chen, X., Li, W., Ren, J., Huang, D., He, W.T., Song, Y., Yang, C., Li, W., Zheng, X., Chen, P., and Han, J. (2014). Translocation of mixed lineage kinase domain-like protein to plasma membrane leads to necrotic cell death. Cell Res. *24*, 105–121.

Cho, Y.S., Challa, S., Moquin, D., Genga, R., Ray, T.D., Guildford, M., and Chan, F.K. (2009). Phosphorylation-driven assembly of the RIP1-RIP3 complex regulates programmed necrosis and virus-induced inflammation. Cell *137*, 1112–1123.

Denning, T.L., Norris, B.A., Medina-Contreras, O., Manicassamy, S., Geem, D., Madan, R., Karp, C.L., and Pulendran, B. (2011). Functional specializations of intestinal dendritic cell and macrophage subsets that control Th17 and regulatory T cell responses are dependent on the T cell/APC ratio, source of mouse strain, and regional localization. J. Immunol. *187*, 733–747.

Diehl, G.E., Longman, R.S., Zhang, J.X., Breart, B., Galan, C., Cuesta, A., Schwab, S.R., and Littman, D.R. (2013). Microbiota restricts trafficking of bacteria to mesenteric lymph nodes by CX(3)CR1(hi) cells. Nature *494*, 116–120.

Dillon, C.P., Oberst, A., Weinlich, R., Janke, L.J., Kang, T.B., Ben-Moshe, T., Mak, T.W., Wallach, D., and Green, D.R. (2012). Survival function of the FADD-CASPASE-8-cFLIP(L) complex. Cell Rep. *1*, 401–407.

Dondelinger, Y., Declercq, W., Montessuit, S., Roelandt, R., Goncalves, A., Bruggeman, I., Hulpiau, P., Weber, K., Sehon, C.A., Marquis, R.W., et al. (2014). MLKL compromises plasma membrane integrity by binding to phosphatidylinositol phosphates. Cell Rep. *7*, 971–981.

Gautheron, J., Vucur, M., Reisinger, F., Cardenas, D.V., Roderburg, C., Koppe, C., Kreggenwinkel, K., Schneider, A.T., Bartneck, M., Neumann, U.P., et al. (2014). A positive feedback loop between RIP3 and JNK controls non-alcoholic steatohepatitis. EMBO Mol. Med. *6*, 1062–1074.

Godwin, A., Sharma, A., Yang, W.L., Wang, Z., Nicastro, J., Coppa, G.F., and Wang, P. (2015). Receptor-interacting protein kinase 3 deficiency delays cutaneous wound healing. PLoS ONE *10*, e0140514.

He, S., Wang, L., Miao, L., Wang, T., Du, F., Zhao, L., and Wang, X. (2009). Receptor interacting protein kinase-3 determines cellular necrotic response to TNF-alpha. Cell *137*, 1100–1111.

He, S., Liang, Y., Shao, F., and Wang, X. (2011). Toll-like receptors activate programmed necrosis in macrophages through a receptor-interacting kinase-3-mediated pathway. Proc. Natl. Acad. Sci. USA *108*, 20054–20059.

He, Y., Franchi, L., and Núñez, G. (2013). TLR agonists stimulate Nlrp3-dependent IL-1β production independently of the purinergic P2X7 receptor in dendritic cells and in vivo. J. Immunol. *190*, 334–339.

Kaczmarek, A., Vandenabeele, P., and Krysko, D.V. (2013). Necroptosis: the release of damage-associated molecular patterns and its physiological relevance. Immunity *38*, 209–223.

Kaiser, W.J., Upton, J.W., Long, A.B., Livingston-Rosanoff, D., Daley-Bauer, L.P., Hakem, R., Caspary, T., and Mocarski, E.S. (2011). RIP3 mediates the embryonic lethality of caspase-8-deficient mice. Nature *471*, 368–372.

Kang, T.B., Yang, S.H., Toth, B., Kovalenko, A., and Wallach, D. (2013). Caspase-8 blocks kinase RIPK3-mediated activation of the NLRP3 inflammasome. Immunity *38*, 27–40.

Kang, S., Fernandes-Alnemri, T., Rogers, C., Mayes, L., Wang, Y., Dillon, C., Roback, L., Kaiser, W., Oberst, A., Sagara, J., et al. (2015). Caspase-8 scaffolding function and MLKL regulate NLRP3 inflammasome activation downstream of TLR3. Nat. Commun. *6*, 7515.

Latz, E., Xiao, T.S., and Stutz, A. (2013). Activation and regulation of the inflammasomes. Nat. Rev. Immunol. *13*, 397–411.

Lawlor, K.E., Khan, N., Mildenhall, A., Gerlic, M., Croker, B.A., D'Cruz, A.A., Hall, C., Kaur Spall, S., Anderton, H., Masters, S.L., et al. (2015). RIPK3 promotes cell death and NLRP3 inflammasome activation in the absence of MLKL. Nat. Commun. *6*, 6282.

Lee, Y., Kumagai, Y., Jang, M.S., Kim, J.H., Yang, B.G., Lee, E.J., Kim, Y.M., Akira, S., and Jang, M.H. (2013). Intestinal Lin- c-Kit+ NKp46- CD4- population strongly produces IL-22 upon IL-1β stimulation. J. Immunol. *190*, 5296–5305.

Lenardo, M., Chan, K.M., Hornung, F., McFarland, H., Siegel, R., Wang, J., and Zheng, L. (1999). Mature T lymphocyte apoptosis–immune regulation in a dynamic and unpredictable antigenic environment. Annu. Rev. Immunol. *17*, 221–253.

Li, J., McQuade, T., Siemer, A.B., Napetschnig, J., Moriwaki, K., Hsiao, Y.S., Damko, E., Moquin, D., Walz, T., McDermott, A., et al. (2012). The RIP1/RIP3 necrosome forms a functional amyloid signaling complex required for programmed necrosis. Cell *150*, 339–350.

Longman, R.S., Diehl, G.E., Victorio, D.A., Huh, J.R., Galan, C., Miraldi, E.R., Swaminath, A., Bonneau, R., Scherl, E.J., and Littman, D.R. (2014). CX_3CR1^+ mononuclear phagocytes support colitis-associated innate lymphoid cell production of IL-22. J. Exp. Med. *211*, 1571–1583.

Mandal, P., Berger, S.B., Pillay, S., Moriwaki, K., Huang, C., Guo, H., Lich, J.D., Finger, J., Kasparcova, V., Votta, B., et al. (2014). RIP3 induces apoptosis independent of pronecrotic kinase activity. Mol. Cell *56*, 481–495.

Manta, C., Heupel, E., Radulovic, K., Rossini, V., Garbi, N., Riedel, C.U., and Niess, J.H. (2013). CX(3)CR1(+) macrophages support IL-22 production by innate lymphoid cells during infection with Citrobacter rodentium. Mucosal Immunol. *6*, 177–188.

McComb, S., Cheung, H.H., Korneluk, R.G., Wang, S., Krishnan, L., and Sad, S. (2012). cIAP1 and cIAP2 limit macrophage necroptosis by inhibiting Rip1 and Rip3 activation. Cell Death Differ. *19*, 1791–1801.

Medina-Contreras, O., Geem, D., Laur, O., Williams, I.R., Lira, S.A., Nusrat, A., Parkos, C.A., and Denning, T.L. (2011). CX3CR1 regulates intestinal macrophage homeostasis, bacterial translocation, and colitogenic Th17 responses in mice. J. Clin. Invest. *121*, 4787–4795.

Moriwaki, K., and Chan, F.K. (2013). RIP3: a molecular switch for necrosis and inflammation. Genes Dev. *27*, 1640–1649.

Moriwaki, K., and Chan, F.K. (2014). Necrosis-dependent and independent signaling of the RIP kinases in inflammation. Cytokine Growth Factor Rev. *25*, 167–174.

Moriwaki, K., and Chan, F.K. (2016). Regulation of RIPK3- and RHIM-dependent necroptosis by the proteasome. J. Biol. Chem. *291*, 5948–5959.

Moriwaki, K., Balaji, S., McQuade, T., Malhotra, N., Kang, J., and Chan, F.K. (2014). The necroptosis adaptor RIPK3 promotes injury-induced cytokine expression and tissue repair. Immunity *41*, 567–578.

Moriwaki, K., Bertin, J., Gough, P.J., and Chan, F.K.M. (2015). A RIPK3-caspase 8 complex mediates atypical pro-IL-1β processing. J. Immunol. *194*, 1938–1944.

Moriwaki, K., Balaji, S., and Chan, F.K. (2016). Border security: the role of RIPK3 in epithelium homeostasis. Front. Cell Dev. Biol. *4*, 70.

Newton, K., Dugger, D.L., Wickliffe, K.E., Kapoor, N., de Almagro, M.C., Vucic, D., Komuves, L., Ferrando, R.E., French, D.M., Webster, J., et al. (2014). Activity of protein kinase RIPK3 determines whether cells die by necroptosis or apoptosis. Science *343*, 1357–1360.

Oberst, A., Dillon, C.P., Weinlich, R., McCormick, L.L., Fitzgerald, P., Pop, C., Hakem, R., Salvesen, G.S., and Green, D.R. (2011). Catalytic activity of the caspase-8-FLIP(L) complex inhibits RIPK3-dependent necrosis. Nature *471*, 363–367.

Scotto-Lavino, E., Du, G., and Frohman, M.A. (2006). 3′ End cDNA amplification using classic RACE. Nat. Protoc. *1*, 2742–2745.

Shih, V.F., Davis-Turak, J., Macal, M., Huang, J.Q., Ponomarenko, J., Kearns, J.D., Yu, T., Fagerlund, R., Asagiri, M., Zuniga, E.I., and Hoffmann, A. (2012). Control of RelB during dendritic cell activation integrates canonical and noncanonical NF-κB pathways. Nat. Immunol. *13*, 1162–1170.

Sun, L., Wang, H., Wang, Z., He, S., Chen, S., Liao, D., Wang, L., Yan, J., Liu, W., Lei, X., and Wang, X. (2012). Mixed lineage kinase domain-like protein mediates necrosis signaling downstream of RIP3 kinase. Cell *148*, 213–227.

Swirski, F.K., Nahrendorf, M., Etzrodt, M., Wildgruber, M., Cortez-Retamozo, V., Panizzi, P., Figueiredo, J.L., Kohler, R.H., Chudnovskiy, A., Waterman, P., et al. (2009). Identification of splenic reservoir monocytes and their deployment to inflammatory sites. Science *325*, 612–616.

Upton, J.W., Kaiser, W.J., and Mocarski, E.S. (2012). DAI/ZBP1/DLM-1 complexes with RIP3 to mediate virus-induced programmed necrosis that is targeted by murine cytomegalovirus vIRA. Cell Host Microbe *11*, 290–297.

Vince, J.E., Wong, W.W., Gentle, I., Lawlor, K.E., Allam, R., O'Reilly, L., Mason, K., Gross, O., Ma, S., Guarda, G., et al. (2012). Inhibitor of apoptosis proteins limit RIP3 kinase-dependent interleukin-1 activation. Immunity *36*, 215–227.

Vitner, E.B., Salomon, R., Farfel-Becker, T., Meshcheriakova, A., Ali, M., Klein, A.D., Platt, F.M., Cox, T.M., and Futerman, A.H. (2014). RIPK3 as a potential therapeutic target for Gaucher's disease. Nat. Med. *20*, 204–208.

Wang, H., Sun, L., Su, L., Rizo, J., Liu, L., Wang, L.F., Wang, F.S., and Wang, X. (2014). Mixed lineage kinase domain-like protein MLKL causes necrotic membrane disruption upon phosphorylation by RIP3. Mol. Cell *54*, 133–146.

Yang, Y., Ma, J., Chen, Y., and Wu, M. (2004). Nucleocytoplasmic shuttling of receptor-interacting protein 3 (RIP3): identification of novel nuclear export and import signals in RIP3. J. Biol. Chem. *279*, 38820–38829.

Yoon, S., Bogdanov, K., Kovalenko, A., and Wallach, D. (2016). Necroptosis is preceded by nuclear translocation of the signaling proteins that induce it. Cell Death Differ. *23*, 253–260.

Zhang, H., Zhou, X., McQuade, T., Li, J., Chan, F.K., and Zhang, J. (2011). Functional complementation between FADD and RIP1 in embryos and lymphocytes. Nature *471*, 373–376.